JOURNAL OF THERMOPHYSICS AND HEAT TRANSFER
Vol. 12, No. 1, January–March 1998

Thermal Design of High-T_c Superconductor Radiometers

Z. M. Zhang*
University of Florida, Gainesville, Florida 32611
and
J. P. Rice† and R. U. Datla‡
National Institute of Standards and Technology, Gaithersburg, Maryland 20899

This paper investigates the feasibility of constructing electrical substitution radiometers operating near liquid-nitrogen temperature using high-temperature (T_c) superconductors. Three design examples that utilize micromachining techniques and a $YBa_2Cu_3O_{7-d}$ superconductor meander line are presented and evaluated. The key performance parameters of a radiometer, such as the power noise level, the maximum measurable power, the time constant, and the spatial uniformity, are predicted based on the design geometry and materials properties. A finite element method is employed to calculate the temperature distribution on the receiver. The temperature responsivity is obtained for different heating methods. The spatial nonuniformity and the nonequivalence between radiative heating and electrical heating are determined. A time constant of about 1 s, a measurable power ranging from 150 nW to 150 μW, and a nonequivalence (between radiative and electrical heating) of 0.36% are predicted for a design that uses a thin silicon substrate sustained by a yttria-stabilized zirconia membrane. A time constant of about 2 s, a measurable power ranging from 1.3 μW to 1.3 mW, and a nonequivalence of 0.18% are predicted for a design that uses a 25-μm-thick sapphire plate.

Nomenclature

A	=	area of the receiver, m^2
C	=	heat capacity of the receiver, J/K
c_p	=	specific heat, J/kg K
d	=	thickness, m
G	=	thermal conductance, W/K
k	=	thermal conductivity, W/m K
l	=	length, m
P	=	radiant or electrical power, W
P_{max}	=	maximum measurable power, W
P_{min}	=	minimum measurable power, W
P_n	=	power noise, W
R	=	temperature responsivity, K/W
T	=	temperature of the receiver, K
T_{av}	=	average temperature of the YBCO meander line, K
T_c	=	critical temperature, K
T_0	=	temperature of the heat sink, K
w	=	width, m
X, Y, Z	=	coordinates, m
ΔT	=	temperature difference ($T - T_0$), K
δT_n	=	temperature noise level, K
ρ	=	density, kg/m^3
σ	=	Stefan–Boltzmann constant, 5.67×10^{-8} W/m^2 K^4
τ	=	time constant (C/G), s

I. Introduction

INFRARED radiometers have many applications, including noncontact temperature measurements and space observations.[1,2] Room-temperature electrical substitution radiometers are commonly used in laboratory and industry measurements.[3] Cryogenic electrical substitution radiometers, operating between 2–5 K using liquid helium, have been used as primary standards for the realization of radiance and irradiance scales.[4–6] There is a need for fast, portable, accurate, and sensitive radiometers that can be used as transfer standards for calibration of commercial radiometers and blackbody sources. These radiometers should operate at liquid-nitrogen temperature (77 K) or higher for low cost and easy operation. By reducing the temperature from room temperature to liquid-nitrogen temperature, the background radiation will decrease by two orders of magnitude. High-T_c superconductors have been used to fabricate sensitive radiation detectors operating above 77 K (Refs. 7 and 8). These devices utilize the strong temperature dependence of the electrical resistance of a superconductive material in the superconducting-to-normal state transition region. Rice and Zhang[9] presented a high-T_c superconductor radiometer design for use as an infrared transfer standard. The spatial uniformity and the nonequivalence between the electrical heating and radiative heating, however, were not predicted.

In the present study, thermal design and modeling are performed to evaluate the feasibility of using high-T_c superconductive films as the temperature sensor for infrared radiometers. The key parameters that are important to the radiometer application are discussed, resulting in a series of design criteria. Three different design structures that utilize state-of-the-art micromachining technology are presented. The temperature distribution at the receiver is predicted using finite element analysis software. The spatial uniformity of the radiometer responsivity is determined. The nonequivalence of the detector responsivity between the electrical heating and the radiative heating is predicted for each design. The time constant, the dynamic range, and the noise level are also calculated.

II. Design Criteria and Structures

A. Parameters and Their Relations

For an electrical substitution radiometer, a temperature sensor and a heater are located on a receiver that is thermally

Received Feb. 12, 1996; revision received May 9, 1997; accepted for publication May 11, 1997.

*Assistant Professor, Department of Mechanical Engineering. Senior Member AIAA.
†Physicist, Optical Materials and Infrared Technology Group of the Optical Technology Division.
‡Supervisory Physicist and Leader, Optical Materials and Infrared Technology Group of the Optical Technology Division.

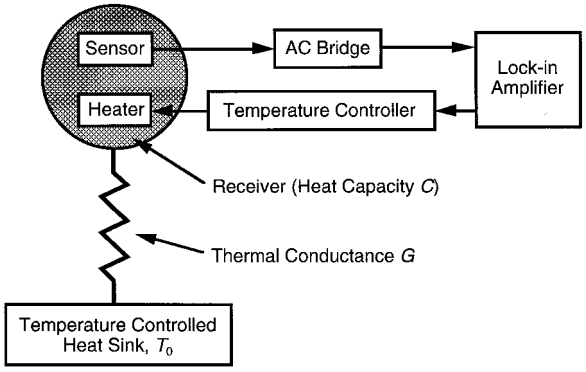

Fig. 1 Schematic of an electrical substitution radiometer.

isolated from a heat sink (Fig. 1). In the active mode of operation, the temperatures of both the heat sink and the receiver are maintained constant using feedback control. A shutter in front of the radiometer (not shown in Fig. 1) can be opened to receive the incoming radiation. The radiative power is the difference in the electrical power supplied to the receiver before and after the shutter is opened. One of the advantages of using electrical substitution is that the nonlinearity caused by either the detector or the amplifier is essentially eliminated.[9] Nonlinearity can be a major source of uncertainty for thermal detectors including high-T_c superconducting bolometers.[10,11]

For use as a transfer standard for optical power measurements, the receiver should be sufficiently large that the beam underfills its sensing area. In a typical application, such as for measuring the power in the monochromator exit beam of the NIST (National Institute of Standards and Technology) Infrared Detector Comparator, the detector is at least 5 mm in diameter.[11] Depending on the particular application, the incoming radiant power level ranges from submicrowatt to a few milliwatts. A large dynamic range (3–5 decades) is also desired. The time constant of absolute radiometers ranges from several seconds to a few minutes.[3,6,12] However, an ambient-background infrared transfer standard radiometer typically must be fast enough that the beam can be chopped to minimize background effects. The time constant τ is determined from the total heat capacity C of the receiver and the thermal conductance G between the receiver and the heat sink by $\tau = C/G$. C is limited by the dimensions and the properties of the materials, mainly the substrate material. The smaller the G, the larger the temperature rise for the same input power (i.e., the temperature responsivity). The minimum measurable power with 1% uncertainty is 100 times the product of G and the temperature noise δT_n; i.e., $P_{\min} = 100G\delta T_n$. Since the voltage and critical current relation of a superconductor can be used to measure the temperature change, a superconducting thermometer can operate below the critical temperature T_c (Refs. 13 and 14). This greatly improves the dynamic range because the transition width of high-T_c materials is usually less than 1 K. If the temperature of the heat sink is maintained at $T_0 = 80$ K, and that of the receiver is maintained at $T = 90$ K, the maximum temperature difference is $\Delta T_{\max} = 10$ K, and the maximum power is $P_{\max} = G\Delta T_{\max}$. The measurable power range (i.e., the dynamic range) is determined by the temperature noise and the maximum allowable temperature difference between the receiver and the heat sink. Assume the temperature noise level is 100 μK based on the experiments of Lesquey et al.[15] Then, G should be $\approx 10^{-5}$ W/K for measurements from 100 nW (with 1% noise) to 100 μW and $\approx 10^{-3}$ W/K for measurements from 10 μW (with 1% noise) to 10 mW. The dynamic range is three decades. Notice that the ultimate limit for the noise equivalent temperature is the phonon noise, which is $\approx 2 \times 10^{-7}$ K Hz$^{-1/2}$ for $G = 10^{-5}$ W/K, and $\approx 2 \times 10^{-8}$ K Hz$^{-1/2}$ for $G = 10^{-3}$ W/K, much smaller than the assumed value of δT_n (Ref. 9). This indicates that the temperature noise can potentially be reduced in the future.

The temperature responsivity is the receiver's temperature rise per unit power supplied to the receiver, either by radiation or by the electrical heater. For radiation incident on different positions of the receiver, the responsivity may be different. The uncertainty associated with the position-dependent responsivity is called spatial nonuniformity. The responsivity may also be different between electrical heating and radiative heating, which is called nonequivalence in radiometry. Detailed information about the temperature distribution on the receiver for each type of heating method is required to determine the nonuniformity and nonequivalence. One of the major efforts of the present work is to calculate the temperature distributions and determine the spatial nonuniformity and nonequivalence. The nonequivalence caused by other mechanisms, such as heating by the electrical leads and the nonunity of the absorptance, however, is not investigated in the present study.

B. Design Structures

Three different geometric configurations, manufacturable using contemporary micromachining technologies, are shown in Fig. 2. Designs A and B employ silicon microfabrication technology. The heat sink and the substrate are crystalline silicon. Design A uses a YSZ (yttria-stabilized zirconia) membrane to support the receiver, whereas design B uses silicon bridges. The area of the receiver is 5 × 5 mm. The YSZ membrane is 10 mm × 10 mm × 200 nm. The YSZ membrane and the silicon bridges conduct heat from the receiver to the heat sink. A YBCO ($YBa_2Cu_3O_{7-\delta}$ superconductor, $T_c \approx 90$ K) film (thickness: $d = 50$ nm) is deposited on a silicon slice and then patterned to form a meander line (width: $w = 30$ μm and length: $l = 7$ mm). Similarly, an electrical heater is patterned on the receiver to relate the radiant power to the electrical power. The heater material is assumed to be Inconel® (an alloy made of 78% Ni, 15% Cr, and 7% Fe). (The use of trade names is for identification only and does not imply endorsement by the National Institute of Standards and Technology, nor does it imply that the materials or products identified are necessarily the best available for the purpose.) Buffer layers are used between the YBCO and Si to grow high-quality superconductive films. Similar structures have been fabricated by several groups, and detailed discussions on the microfabrication aspects can be found in the literature.[16–20] Four 1 mm × 1 mm Au pads are deposited on the receiver to connect the electrical leads to the heaters and YBCO (Fig. 3).

Design C uses a sapphire plate (25 μm thick) as the substrate for the receiver, which is supported by Kevlar® threads. A superconductive YBCO film and a heater are deposited and patterned on the sapphire substrate. The thermal coupling between the receiver and the copper heat sink is through eight Au wires (18 μm in diameter and 6 mm long). Brasunas and Lakew[21] fabricated a superconducting bolometer on a sapphire substrate and obtained a peak detectivity of 6×10^9 cm Hz$^{1/2}$ W^{-1} at 90 K with a chopping frequency near 4 Hz. This result is comparable to the best performance of existing thermal detectors operated above the liquid-nitrogen temperature.

For all three designs, the YBCO and the heater are patterned on the back surface. It is assumed that the front surface is coated with an absorption layer (such as Au black), since the infrared absorptance of ≈ 0.5 that is achievable with high-T_c superconducting films is too low for transfer standard radiometers.[8,22,23] The wavelength region of interest for using a high-T_c radiometer is between 2–20 μm, where the absorptance of Au black is close to unity.[22] Furthermore, a hemispherical mirror may be used to enhance the absorptance.[9,24,25] Considering an Au black coating with an area density of 80 μg/cm^2 and using the specific heat of gold,[22] the heat capacity of the coating at 90 K will be ≈ 2 μJ/K, which is 13% of the total heat capacity of the receiver for design A, 2% for design B, and 1% for design C. Because the thickness and thermophysical properties of Au black depend on deposition conditions, the heat capacity of the coating is neglected in the present study.

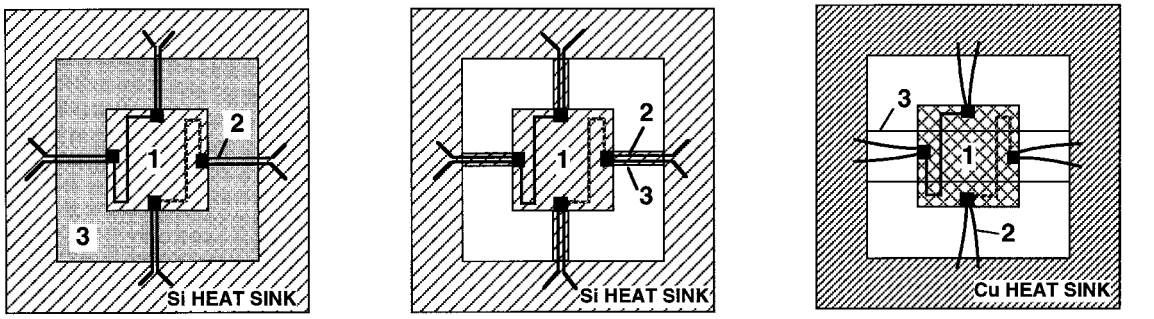

Fig. 2 Three different designs of high-T_c superconductor radiometers, where the outside dimensions of the heat sink are 15 3 15 mm.

III. Thermal Modeling

Thermal modeling and analysis are important to the understanding of the mechanisms of superconducting bolometric and nonequilibrium responses.[8,26–28] In the present study, a commercial finite element software is used to obtain the temperature distribution. The finite element method, software, and hardware used in the present study have been discussed in previous publications.[12,29] At steady state, the temperature difference in the Z direction is negligibly small compared to that in the X and Y directions. (The influence of the temperature gradient inside the coating will be discussed in Sec. IV). Hence, the substrate, the Au pads, and the YSZ membrane are treated as surface elements, stacked on each other. The mesh on the receiver is shown in Fig. 3. Each element is 0.25 × 0.25 mm. The YBCO, Inconel, and Au leads are modeled using line elements. The total number of elements is 2564 for design A, 1004 for design B, and 972 for design C. The steady-state computation takes only a few minutes of CPU time on a workstation with a speed of 125-million floating-point operations per second.

The numerical code used for this work cannot provide an error estimate for elements that involve mixed materials and radiation heat exchange. Therefore, careful checks are performed to assure validity of the numerical model. First, simplified models are developed with constant thermophysical properties and no radiation. Assuming that the temperature at the receiver is uniform (using a very large thermal conductivity), the simulated results agree with analytical solutions within the convergence criterion of 1 μK. Second, previous studies have shown that the modeling results agree well with experiments and analytical solutions for different types of radiometers.[12,29] Third, comparisons are made with different number of elements and element size. By increasing the number of elements on the receiver from 20 × 20 to 40 × 40, the calculated temperature of any node changes less than 0.4%. The change in the predicted nonequivalence is less than 1% because a systematic error in the temperature change does not significantly affect the nonequivalence. The purpose of this paper is to demonstrate the feasibility of constructing radiometers operating above liquid-nitrogen temperature using high-T_c superconductors. Considering the uncertainty in the determination of thermophysical properties, no further mesh refinement is performed.

Since the radiometer must operate in an evacuated chamber to avoid water condensation, convective heat transfer and gas

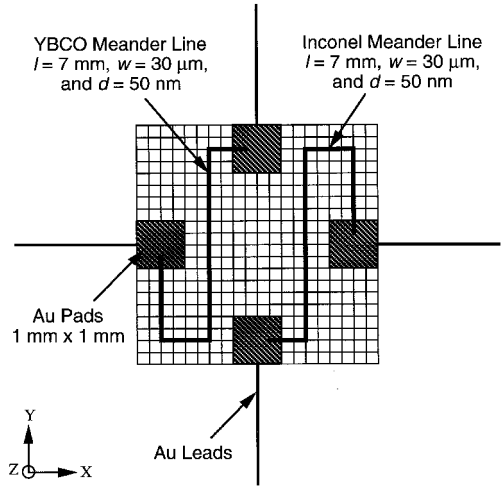

Fig. 3 Illustration of the mesh on the 5 3 5 mm receiver.

conduction can be neglected. If the emissivity for both sides of the receiver is 1, the thermal conductance between the receiver and its surroundings via radiation is $\approx 6 \times 10^{-6}$ W/K, which is about 40% of the total thermal conductance for design A, 0.6% for design B, and 5% for design C. Therefore, radiative heat transfer is included in the modeling. The view factor between the receiver and its surroundings is assumed to be 1, and the emissivity of the receiver is taken to be 1 for simplification. The temperature of the surroundings is assumed to be constant and equal to the heat sink temperature T_0. Without any power supply, the receiver temperature would be T_0 everywhere. Radiation and electrical heating are modeled as constant surface heat flux or nodal heating power. The temperature distribution on the receiver depends on the heating location. The nonequivalence is not proportional to the temperature difference on the receiver. Assuming that the electrical output of the YBCO sensor is proportional to the average temperature (T_{av}) of the nodes covered by the YBCO meander line, as shown in Fig. 3, the steady-state responsivity is the average temperature difference ($\Delta T_{av} = T_{av} - T_0$) divided by the input power (P), i.e.,

$$R = \Delta T_{av}/P \tag{1}$$

The difference in R for the same power P supplied to different locations of the receiver is a measure of the spatial nonuniformity. The difference in R between simulated radiative heating and electrical heating determines the nonequivalence. If the temperature difference on the receiver is small compared with that between the receiver and the heat sink, then $R = 1/G$ at a steady state or at chopping frequencies much lower than $1/\tau$. In practice, the temperature of the receiver is actively controlled near the middle point of the superconducting-to-normal state transition of the YBCO sensor. In most cases, the maximum temperature difference along the YBCO meander line is less than 1% ΔT_{av}, i.e., 0.1 K with the maximum heating power. The transition width of the best YBCO films is approximately 0.5 K, and becomes broader for films of lower quality. Therefore, the assumption that the electrical resistivity of YBCO is proportional to temperature is valid except for extreme cases, as discussed in the following section.

IV. Results and Discussion

Table 1 lists the thermophysical properties of the materials used in the designs. All data are from Touloukian and Ho,[30] except that the properties of YBCO are from Flik et al.[26] and the thermal conductivity of YSZ is from Ackerman et al.[31] Because the specific heat data of YSZ below 100 K are not available, the data of ZrO_2 are used instead.[30] By assuming that the receiver is at a uniform temperature, a simple analysis was used to determine the thermal conductance between the receiver and the heat sink. The results agree with those calculated by the numerical model. The detailed temperature distribution, however, cannot be obtained without numerical modeling. Since the maximum temperature difference on the receiver is one to two orders of magnitude smaller than the temperature difference between the receiver and the heat sink, the receiver can be treated as a lumped-capacitance system for the prediction of the transient behavior. The heat capacity of the receiver for each design at 90 K is listed in Table 2, together with other parameters.

The temperature distribution for design A with $P = 50$ μW is shown in Fig. 4 for three different heating methods. The temperature of the heat sink and the surroundings is 80 K. In Figs. 4a and 4b, a constant heat flux is provided to an area of 0.5×0.5 mm at the center and a corner, respectively, to simulate laser heating. In Fig. 4c, heating power is provided on the nodes covered by the Inconel meander line to simulate electrical heating. The average temperature of the YBCO sensor (relative to that of the heat sink) for Figs. 4a–4c is ΔT_{av} = 3.2957, 3.2908, and 3.2922 K, respectively. The maximum temperature difference on the receiver for Figs. 4a and 4c is $\approx$0.5% ΔT_{av}, whereas that for Fig. 4b is $\approx$1% ΔT_{av}. The relative difference in responsivity for Figs. 4a–4c is 0.15%. However, if the heat flux is supplied to the lower corner (X = 0.25–0.75 mm; Y = 0.25–0.75 mm), then ΔT_{av} = 3.3025 K. The difference in ΔT_{av} or R between heating at the upper corner and the lower corner is $\approx$0.35%. The minimum sensing temperature is found when the heat flux is provided at the middle along an edge (X = 4.25–4.75 mm; Y = 2.25–2.75

Table 1 Properties of materials used in the designs[26,30,31]

T, K	Au	Inconel	Sapphire	Si	YBCO	YSZ
			k, W/m K			
75	355	11.8	1250	1510	9.97	1.62
80	352	11.9	960	1340	9.65	1.68
85	350	12.0	800	1210	9.33	1.74
90	348	12.1	640	1080	9.02	1.80
95	347	12.2	545	982	8.70	1.85
			c_p, J/kg K			
75	97	273	56	169	152	95
80	100	277	68	188	163	107
85	102	281	81	206	175	118
90	104	286	95	224	186	130
95	106	290	110	241	198	142
			ρ, kg/m^3			
——	19,300	8600	4000	2300	6350	5200

Table 2 Predicted performance parameters of three different designs for a maximum temperature difference ΔT_{max} = 10 K

	Design		
	A	B	C
G, mW/K	0.015	0.96	0.13
C at 90 K, mJ/K	0.016	0.13	0.24
τ, s	1.1	0.14	1.8
$R = 1/G$, K/mW	67	1.04	7.7
$P_{max} = G\Delta T_{max}$, mW	0.15	10	1.3
δT_n, μK	<100	<100	<100
$P_n = G\delta T_n$, nW	<1.5	<100	<13
Spatial nonuniformity and/or nonequivalence	<0.4%	<3%	<0.2%

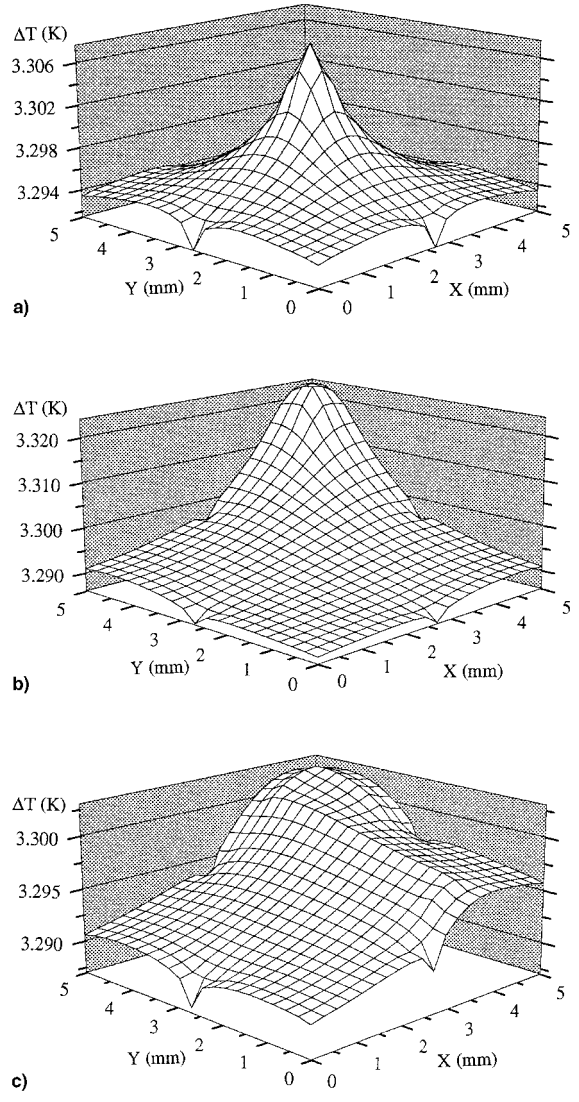

Fig. 4 Temperature distribution on the receiver for design A, where the total heating power is 50 μW and the heat sink temperature T_0 = 80 K: a) radiative heating at the center (X = 2.25–2.75 mm; Y = 2.25–2.75 mm); b) radiative heating at the upper-right corner (X = 4.25–4.75 mm; Y = 4.25–4.75 mm); and c) electrical heating at nodes defined by the Inconel film.

mm), with ΔT_{av} = 3.2906 K. The maximum spatial nonuniformity is ≈0.36%. The nonequivalence between electrical heating and radiative heating is ≈0.31%. If the YBCO film covers the whole sensing area, then ΔT_{av} will be the average temperature of the receiver. In this case, the maximum nonuniformity is reduced to 0.03%. The thermal conductance calculated by $G = P/\Delta T_{av}$ is ≈15 μW/K, and the time constant is ≈1 s.

Table 2 lists the predicted parameters for all three designs. For design A, the responsivity and thermal conductance are calculated with T_0 = 80 K and P = 50 μW. The responsivity may vary up to 7% because of the temperature dependence of the thermal conductivity of YSZ and the nonlinear temperature dependence of radiative heat transfer. For design B, the listed responsivity is calculated with T_0 = 80 K and P = 1 mW, which may vary up to 20% because the thermal conductivity of Si depends strongly on temperature. The responsivity for design C changes little because of the nearly constant thermal conductivity of the Au wires. The uncertainty in the numerical calculation of the responsivity and thermal conductance is estimated to be 0.5% (using a coverage factor of 2, i.e., 95% confidence). The predicted spatial nonuniformity and/or nonequivalence listed in Table 2 are conservative estimates for the worst case. The noise power is 1.5 nW for design A, which is much lower than that for any room-temperature electrical substitution radiometers, including the pyroelectric detector.[3,24]

The receiver temperature distribution for design B is shown in Fig. 5 for a total power P = 1 mW. In Fig. 5a, the heating power is provided on the middle along an edge to show the effect of applying power near one of the bridges; simulation of laser heating at the center was also performed for design B. The responsivity is about 1 K/mW, which is much smaller than that of design A because of the high thermal conductivity of silicon. Even though the substrate thickness of design B is 10 times that of design A, the spatial uniformity is much worse. The maximum temperature difference on the receiver in Fig. 5b is ≈0.1 K, nearly 10% of the temperature difference between the receiver and the heat sink. In the worst case, the maximum temperature difference on the YBCO meander line is 0.07 K. For power greater than 1 mW, the large temperature difference on the YBCO meander line may invalidate the assumption that the electrical resistivity of YBCO is proportional to temperature. The spatial nonuniformity and nonequivalence calculated from the mean temperature of the YBCO meander line is 2.7%, as listed in Table 2. Because the spatial nonuniformity is beyond the desired range, two methods are suggested to improve the nonuniformity of design B. One method is to increase the thickness of the silicon substrate to 40 μm to reduce the nonuniformity to less than 1%. The heat capacity and the time constant would be increased by a factor of 4, which is still less than 1 s. Although design B is not as sensitive as design A, it may be suitable for high-power (near 1 mW) applications. The second method is to increase the length of the Si bridges, which will increase both the uniformity and the responsivity but will decrease the speed. The feasibility of using longer bridges to hold a large mass merits further investigation.

The modeling shows that design C has a better spatial uniformity, a slightly larger time constant, and about an order of magnitude smaller responsivity than design A (see Table 2). The measurable power range is comparable with a high-accuracy cryogenic radiometer currently used for laser power calibration at the National Institute of Standards and Technology, Gaithersburg, Maryland.[6] Therefore, design C is a promising option for construction of transfer standard radiometers with a measurable power ranging from 1.3 μW to 1.3 mW.

For Au black, the density is as low as 3/1000 of that of bulk gold, and the reported electrical conductivity is much lower than shiny Au film.[22] Hence, the thermal conductivity would be much lower than bulk gold. A thickness of ≥10 μm is required to achieve a high absorptivity. Therefore, the temperature gradient across the coating could be comparable with the temperature gradient in the X-Y plane of the receiver. Because radiation is absorbed inside the coating, but the electrical heater is underneath the coating, the temperature distributions are different for radiative and electrical heating. However, if radiative heat loss is small compared to heat conduction, the temperature of the YBCO film will be approximately the same for radiative and electrical heating with the same power.[12] For design A, the radiative heat loss is comparable to the heat conduction. Therefore, the effect of the temperature gradient in the coating is evaluated next.

Assuming that the temperature of the silicon substrate is uniform and that all the radiation is absorbed by or emitted from the surface, a thermal circuit is illustrated in Fig. 6, where G_1 and G_2 represent the thermal conductance across the coating and that between the receiver and the heat sink by conduction,

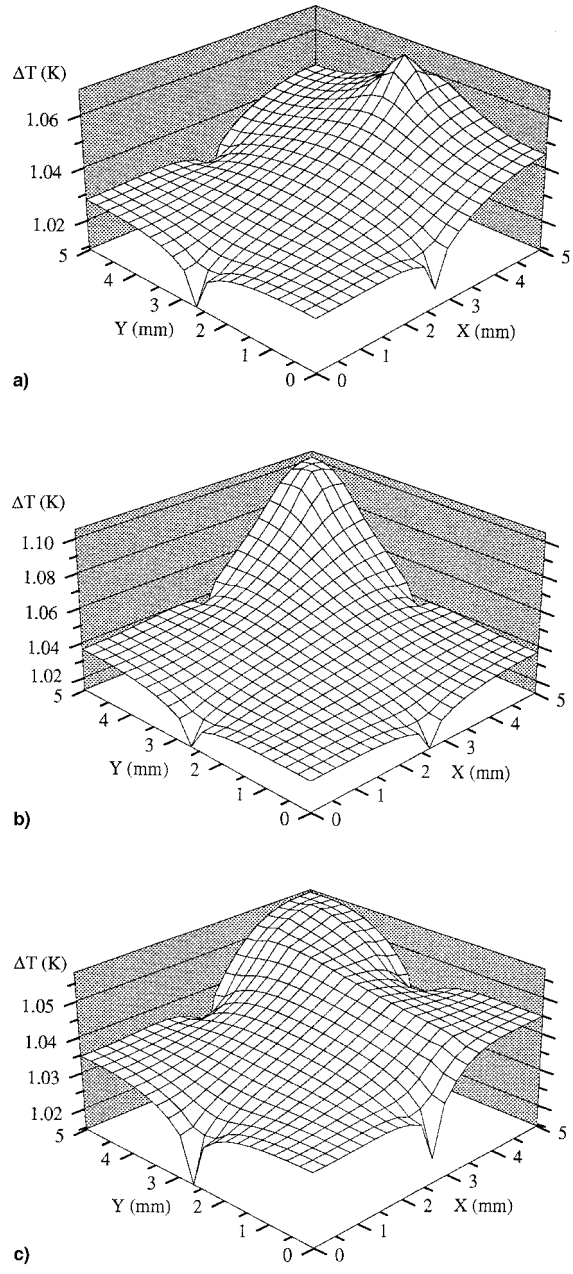

Fig. 5 Temperature distribution on the receiver for design B, where the total heating power is 1 mW and the heat sink temperature T_0 = 80 K: a) radiative heating at middle of the right edge (X = 4.25–4.75 mm; Y = 2.25–2.75 mm); b) radiative heating at the upper-right corner (X = 4.25–4.75 mm; Y = 4.25–4.75 mm); and c) electrical heating at nodes defined by the Inconel film.

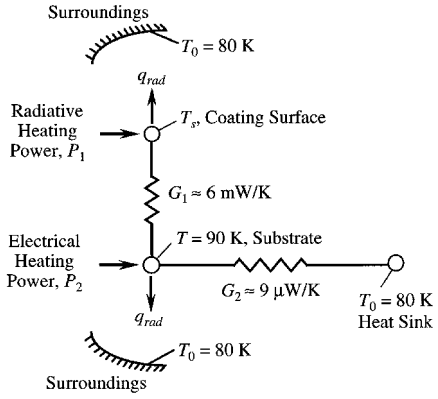

Fig. 6 Thermal circuit for evaluation of the effect of the temperature gradient in the coating on the nonequivalence.

T_s and T are the temperatures of the coating surface and the substrate, respectively, and P_1 and P_2 indicate different heating methods. The steady-state energy balance equations are

$$P_1 - G_1(T_s - T) - \sigma A(T_s^4 - T_0^4) = 0 \quad (2)$$

$$P_2 + G_1(T_s - T) - \sigma A(T^4 - T_0^4) - G_2(T - T_0) = 0 \quad (3)$$

Assume that the gold black is 15 μm thick with a thermal conductivity of 0.35 W/m K (1/1000 that of bulk gold) and has an effective cross-sectional area of 0.25 mm^2 (the laser beam spot size). G_1 is calculated to be $\approx$6 mW/K. Taking T = 90 K and T_0 = 80 K, G_2 is estimated to be $\approx$9 μW/K. P_2 and T_s can be solved from Eqs. (2) and (3) by setting P_1 = 0; i.e., P_2 = 0.15986 mW and $T_s - T = -5.82$ mK. Similarly, P_1 and T_s can be solved from Eqs. (2) and (3) by setting P_2 = 0; i.e., P_1 = 0.15997 mW and $T_s - T$ = 20.82 mK. The nonequivalence in power is $|(P_1 - P_2)/P_2| \approx 0.07\%$. Hence, the temperature gradient inside the coating has little effect on the nonequivalence.

V. Concluding Remarks

This paper presents three design examples of electrical substitution radiometers operating above 77 K, based on a high-T_c superconductor temperature sensor and silicon or sapphire micromachining techniques. A detailed thermal modeling is performed for each design using a finite element method. The performance parameters are predicted according to the geometry and thermophysical properties of the materials. The steady-state temperature distribution on the receiver is obtained for different heating methods. The spatial uniformity and the nonequivalence between radiative heating and electrical heating are evaluated. This work demonstrates the feasibility of fabricating superconducting radiometers with a time constant on the order of 1 s, noise powers from 1.5 to 100 nW, maximum measurable powers from 150 μW to 10 mW, a dynamic range of three decades, and a spatial uniformity of better than 1%. These results suggest that high-T_c superconductor radiometers can outperform room-temperature electrical substitution radiometers in terms of the response time, the minimum measurable power, and the dynamic range. This study will facilitate the development of electrical substitution radiometers using high-T_c superconducting materials. Furthermore, the thermal design method may also be used to analyze and design other types of radiometers. Future experimental research is required to realize these devices.

Acknowledgments

Z.M.Z. acknowledges the support of the University of Florida via an Interdisciplinary Research Initiative award and of the National Institute of Standards and Technology via an Intergovernmental Personnel Act agreement. The authors are grateful to H. C. Tang for his technical support in the use of the finite element analysis software, and to S. R. Lorentz for his insightful comments. The authors acknowledge K. S. Harshavardhan, Neocera, College Park, Maryland, for demonstrating the feasibility of integrating a YBCO temperature sensor and an Inconel heater on a sapphire substrate. Presented as Paper 96-3961 at the National Heat Transfer Conference, Houston, Texas, Aug. 3–6, 1996.

References

[1]McCreight, C. R., Estrada, J. A., Goebel, J. H., McKelvey, M. E., McKibbin, D. D., McMurray, R. E., Jr., Weber, T. T., Farhoomand, J., Moss, N. N., and Savage, M. L., "Low-Background Detector Arrays for Infrared Astronomy," *Proceedings of the Society of Photo-Optical Instrumentation Engineers*, Vol. 973, 1988, pp. 250–255.

[2]Mahan, J. R., Tira, N. E., Lee, R. B., and Keynton, R. J., "Comparison of the Measured and Predicted Response of the Earth Radiation Budget Experiment Active Cavity Radiometer During Solar Observations," *Applied Optics*, Vol. 28, No. 7, 1989, pp. 1327–1337.

[3]Hengstberger, F. (ed.), *Absolute Radiometry: Electrically Calibrated Thermal Detectors of Optical Radiation*, Academic, Boston, MA, 1989.

[4]Martin, J. E., Fox, N. P., and Key, P. J., "A Cryogenic Radiometer for Absolute Radiometric Measurements," *Metrologia*, Vol. 21, No. 5, 1985, pp. 147–155.

[5]Datla, R. U., Stock, K., Parr, A. C., Hoyt, C. C., Miller, P. J., and Foukal, P. V., "Characterization of an Absolute Cryogenic Radiometer (ACR) as a Standard Detector for Radiant Power Measurements," *Applied Optics*, Vol. 31, No. 34, 1992, pp. 7219–7225.

[6]Houston, J. M., Cromer, C. L., Hardis, J. E., and Larason, T. C., "Comparison of the NIST High Accuracy Cryogenic Radiometer and the NIST Scale of Detector Spectral Response," *Metrologia*, Vol. 30, No. 4, 1993, pp. 285–290.

[7]Richards, P. L., "Bolometers for Infrared and Millimeter Waves," *Journal of Applied Physics*, Vol. 76, No. 1, 1994, pp. 1–24.

[8]Zhang, Z. M., and Frenkel, A., "Thermal and Nonequilibrium Responses of Superconductors for Radiation Detectors," *Journal of Superconductivity*, Vol. 7, No. 6, 1994, pp. 871–884.

[9]Rice, J. P., and Zhang, Z. M., *Liquid-Nitrogen-Cooled High T_c Electrical Substitution Radiometer as a Broadband IR Transfer Standard*, NIST TN 1414, U.S. Government Printing Office, Washington, DC, 1996.

[10]Epifani, M., "Nonlinearity Effects in High-Temperature Superconducting Bolometers," *Journal of Applied Physics*, Vol. 76, No. 2, 1994, pp. 1256–1259.

[11]Eppeldauer, G., Migdall, A. L., and Cromer, C. L., "A Cryogenic Silicon Resistance Bolometer for Use as an Infrared Transfer Standard Detector," *Thermal Phenomena at Molecular and Microscales and in Cryogenic Infrared Detectors*, edited by M. Kaviany et al., American Society of Mechanical Engineers, HTD, Vol. 277, New York, 1994, pp. 63–67.

[12]Zhang, Z. M., Datla, R. U., Lorentz, S. R., and Tang, H. C., "Thermal Modeling of Absolute Cryogenic Radiometers," *Journal of Heat Transfer*, Vol. 116, No. 4, 1994, pp. 993–998.

[13]Flik, M. I., Zhang, Z. M., and Goodson, K. E., "Intrinsic Superconducting Radiation Detector," *Applied Physics Letters*, Vol. 62, No. 22, 1993, pp. 2862–2864.

[14]Langlois, P., Robbes, D., Sing, M. L. C., Gunther, C., Bloyet, D., Hamet, J. F., Desfeux, R., and Murray, H., "Superconducting Fast Microbolometers Operating Below Their Critical Temperature," *Journal of Applied Physics*, Vol. 76, No. 6, 1994, pp. 3858–3868.

[15]Lesquey, E., Gunther, C., Flament, S., Desfeux, R., Hamet, J. F., and Robbes, D., "Progress Toward a Low-Noise Temperature Regulation Using a Superconductive High-T_c Microbridge," *IEEE Transactions on Applied Superconductivity*, Vol. 5, No. 2, 1995, pp. 2427–2430.

[16]Downey, P. M., Jeffries, A. D., Meyer, S. S., Weiss, R., Bachner, F. J., Donnelly, J. P., Lindley, W. T., Mountain, R. W., and Silversmith, D. J., "Monolithic Silicon Bolometers," *Applied Optics*, Vol. 23, No. 6, 1984, pp. 910–914.

[17]Bang, C. B., Rice, J. P., Flik, M. I., Rudman, D. A., and Schmidt, M. A., "Thermal Isolation of High-Temperature Superconducting Thin Films Using Silicon Wafer Bonding and Micromachining," *Journal of Microelectromechanical Systems*, Vol. 2, No. 4, 1993, pp. 160–164.

[18]Li, Q., Fenner, D. B., Hamblen, W. D., and Hamblen, D. G., "Epitaxial $YBa_2Cu_3O_{7-y}$ Bolometers on Micromachined Windows," *Applied Physics Letters*, Vol. 62, No. 19, 1993, pp. 2428–2430.

[19]Johnson, B. R., Foote, M. C., Harsh, H. A., and Hunt, B. D., "Epitaxial $YBa_2Cu_3O_7$ Superconducting Infrared Microbolometers on Silicon," *Proceedings of the Society of Photo-Optical Instrumentation Engineers*, Vol. 2267, 1994, pp. 24–30.

[20]Rice, J. P., Grossman, E. N., and Rudman, D. A., "Antenna-Coupled High-T_c Air-Bridge Microbolometer on Silicon," *Applied Physics Letters*, Vol. 65, No. 6, 1994, pp. 773–775.

[21]Brasunas, J. C., and Lakew, B., "High T_c Superconductor Bolometer with Record Performance," *Applied Physics Letters*, Vol. 64, No. 6, 1994, pp. 777–778.

[22]Advena, D. J., Bly, V. T., and Cox, J. T., "Deposition and Characterization of Far-Infrared Absorbing Gold Black Films," *Applied Optics*, Vol. 32, No. 7, 1993, pp. 1136–1144.

[23]Zhang, Z. M., and Flik, M. I., "Predicted Absorptance of $YBa_2Cu_3O_7$/YSZ/Si Multilayer Structures for Infrared Detectors," *IEEE Transactions on Applied Superconductivity*, Vol. 3, No. 1, 1993, pp. 1604–1607.

[24]Day, G. W., Hamilton, C. A., and Pyatt, K. W., "Spectral Reference Detector for the Visible to 12-μm Region; Convenient, Spectrally Flat," *Applied Optics*, Vol. 15, No. 7, 1976, pp. 1865–1868.

[25]Zhang, Z. M., Ge, X. S., and Wang, Y. F., "A Novel Pyrheliometer of High Accuracy," *Solar Energy*, Vol. 39, No. 5, 1987, pp. 371–377.

[26]Flik, M. I., Phelan, P. E., and Tien, C. L., "Thermal Model for the Bolometric Response of High T_c Superconducting Films to Optical Pulses," *Cryogenics*, Vol. 30, No. 6, 1990, pp. 1118–1128.

[27]Berg, M., Laukemper, J., Neff, H., Steinbeiß, E., Michalke, W., Burnus, M., and Heidenblut, T., "Thermal Budget Simulations and Device Performance of Microstructured High-T_c Transition Edge Bolometers on Silicon," *IEEE Transactions on Applied Superconductivity*, Vol. 5, No. 2, 1995, pp. 2435–2438.

[28]Phelan, P. E., "Thermal Response of Thin-Film High-T_c Superconductors to Modulated Irradiation," *Journal of Thermophysics and Heat Transfer*, Vol. 9, No. 3, 1995, pp. 397–402.

[29]Zhang, Z. M., Livigni, D. J., Jones, R. D., and Scott, T. R., "Thermal Modeling and Analysis of Laser Calorimeters," *Journal of Thermophysics and Heat Transfer*, Vol. 10, No. 2, 1996, pp. 350–356.

[30]Touloukian, Y. S., and Ho, C. Y. (eds.), *Thermophysical Properties of Matter*, Vol. 1, p. 137 for Au, p. 339 for Si, and pp. 1017–1027 for Inconel; Vol. 2, pp. 93–97 for sapphire; Vol. 4, pp. 83–86 for Au, pp. 204–207 for Si, and pp. 553–555 for Inconel; Vol. 5, pp. 24–29 for sapphire, and pp. 293–295 for ZrO_2, IFI/Plenum, New York, 1970.

[31]Ackerman, D. A., Moy, D., Potter, R. C., Anderson, A. C., and Lawless, W. N., "Glassy Behavior of Crystalline Solids at Low Temperatures," *Physical Review B*, Vol. 23, No. 8, 1981, pp. 3886–3893.